



LJMU Research Online

Ahuir-Torres, JI and Sharp, MC

Influence of Pulse Energy and a Material's Magnetic Field on the Morphology of the Dimples Produced with Nanosecond Pulsed Laser on a Magnet

<http://researchonline.ljmu.ac.uk/id/eprint/17350/>

Article

Citation (please note it is advisable to refer to the publisher's version if you intend to cite from this work)

Ahuir-Torres, JI and Sharp, MC (2022) Influence of Pulse Energy and a Material's Magnetic Field on the Morphology of the Dimples Produced with Nanosecond Pulsed Laser on a Magnet. Lasers in Manufacturing and Materials Processing. ISSN 2196-7229

LJMU has developed [LJMU Research Online](#) for users to access the research output of the University more effectively. Copyright © and Moral Rights for the papers on this site are retained by the individual authors and/or other copyright owners. Users may download and/or print one copy of any article(s) in LJMU Research Online to facilitate their private study or for non-commercial research. You may not engage in further distribution of the material or use it for any profit-making activities or any commercial gain.

The version presented here may differ from the published version or from the version of the record. Please see the repository URL above for details on accessing the published version and note that access may require a subscription.

For more information please contact researchonline@ljmu.ac.uk

<http://researchonline.ljmu.ac.uk/>



Influence of Pulse Energy and a Material's Magnetic Field on the Morphology of the Dimples Produced with Nanosecond Pulsed Laser on a Magnet

J. I. Ahuir-Torres¹ · M. C. Sharp¹

Accepted: 20 June 2022
© The Author(s) 2022

Abstract

Magnets made of NdFeB alloys are applied in numerous industries because they have excellent magnetic properties and good thermal stability. However, their low corrosion resistance and fragility reduce the number of the applications in harsh environments. Laser surface texturing is a powerful technique to improve the properties of materials via surface functionalisation. The characteristics of the textures define the properties of the functionalised surfaces and the laser parameters in turn influence the texture features. Pulse energy is a laser parameter with high influence on the geometry and the morphology of the textures. The magnetic field of these magnets are also expected to have an influence on the texture features. In this present work, the influence of the pulse energy (from 5 μ J to 696 μ J) on the dimple characteristics created with an infrared (1064 nm) nanosecond pulsed (200ns) fibre laser single pulses on NdFeB alloy (magnetic material) have been studied. The shape features of the laser textures on the samples were analysed through optical microscopy and profilometry. This work shows that the single pulses produced textures of U-type dimple kind on the metallic material. The shapes of the dimples were also altered by magnetic field of the material, which indicates that the magnetic properties of the alloys remain in liquid state. The factors of the laser beam-material interaction, pulse energy and energy depth penetration, are furthermore presented in this paper. These factors can be employed to design the width, diameter and depth of the dimples.

Keywords Magnet · Laser surface texturing · Pulse energy · Nanosecond pulsed laser · Energy threshold and energy depth penetration

✉ J. I. Ahuir-Torres
j.i.ahuirtorres@ljmu.ac.uk

¹ General Engineering Research Institute, Faculty of Engineering and Technology, Liverpool John Moores University, Byrom Street, L3 3AF Liverpool, United Kingdom

Introduction

The magnetic NdFeB alloys are widely used in many industries, such as wind energy, computer, electronic, telecommunications, consumer and automotive [1–3]. This is due to its excellent intrinsic properties e.g., high energy of production (512 kJ/m^3) [1, 4], lightweight, great coercivity [2, 4], high remanence [4], excellent thermal stability [1, 2], low cost [1], variable lifetime [1] and recyclability [1, 2, 4–6]. This material nevertheless has certain disadvantages such as, low corrosion resistance [4, 6, 7], which diminish the number of its applications.

Surface texturing is a treatment that can improve a number of properties via the functionalisation of the surfaces. This process can be carried out by mean of various methods; e.g., electromechanical machining, chemical etching, plasma, laser and ion beam. Laser Surface Texturing (LST) stands out among them because of its advantages such as, fast, environmentally friendly, automatable, high reproducibility and accuracy [8–10].

The properties of the processed surfaces are defined by the texture characteristics (e.g. width, diameter, depth and average roughness) [11, 12]. These features are, in turn, determined by the laser parameters (wavelength, pulse length, pulse numbers per shot and pulse energy) and the optical and thermodynamic properties of the material [11, 13]. The textures on metallic materials are produced by thermal process for lasers with infrared (IR) wavelengths (λ). The laser radiation is absorbed by free electrons that subsequently collide with lattice phonons. These collisions convert the absorbed laser energy to heat, which can melt and vaporise the material [14, 15]. Then, the laser treated zone is rapidly cooled by the thermal diffusion of the heat in the material. This is the process responsible to generate the textures [10]. In addition, the heat diffusion into material causes a damaged area round the texture that is often called as Heat Affected Zone (HAZ) and commonly impoverishes the texture quality [16, 17]. HAZ thickness is proportional to the square root of the pulse length of the laser (τ) multiplied by the thermal diffusion of the material (κ). The nanosecond pulsed lasers are commonly employed in LST because they produce small HAZ [17]. The amount of material vaporised by the laser beam is highly influenced by pulse energy (E_p). The size of the texture is commonly proportional to vaporised material amount and therefore, it also is proportional to E_p [18]. However, a plasma can be generated at high E_p and short pulse length, τ , which can reduce the LST efficiency. Part of the laser radiation can be absorbed by evaporated material that can become plasma at certain values of E_p and τ . The plasma can absorb, scatter and reflect the laser beam that arrives on the surface of the material. This diminishes the laser radiation amount that reaches on surface and therefore the energy absorbed at the surface is reduced. This effect is usually named as plasma shielding effect [19–21]. Single shot mode is recommendable for texturing because the probability of the plasma shielding effect generation is increased with an increase of the number of pulses hitting a point on the surface (N) [21, 22]. Thus, the pulse energy, E_p , of the single shots is a great important factor on LST.

Note, the NdFeB alloy is a magnetic material whose magnetic field can disturb the quality of the texture. The dispersion of the vaporised material and the hydrodynamic movements of the molten material define the features of the textures. The dispersion

Table 1 Nd-Fe-B magnet chemical composition in percentage by weight

Element	Fe	Nd/PrNd	B	Nb	Dy	Cu
Percentage by weight (%)	66.45	32.00	1.00	0.20	0.10	0.25

and the liquid movements can be hindered by the magnetic field of the solid material because it produces opposite forces to direction to these processes. This is due to the interaction of the magnet's field and the vaporised and molten metallic alloys, [23–25].

Although several researchers have studied the influence of the laser parameters on texture features for metallic materials [26–28], the influence of E_p on texture characteristics on NdFeB alloy has scarcely been reported in the literature. For this reason, the present work is a study about the influence of E_p on the texture features generated via single pulses of a nanosecond pulsed (200ns) IR (1064 nm) fibre laser on a NdFeB alloy magnet. The texture quality is also analysed in this study to assess the influence of the magnetic field of the NdFeB alloy on the laser surface texturing process. The textures produced with single shot were dimples that were analysed through optical light microscopy and profilometry. The study showed that the geometry of the dimples on NdFeB alloy had acceptable quality. The dimple shape was U-type [29–32]. Moreover, the factors of the laser beam-material interaction (energy depth penetration, pulse energy and energy fluence threshold) have been measured in this study. These factors allow selection of laser parameters to create a dimple of a given diameter and depth.

Experimental Setup

Materials and pre-treatment

The magnet used is a N42 neodymium-iron-boron (Nd-Fe-B) magnet, type *F646-1* supplied by *Magnet Expert*. The size of the samples was 20 mm diameter and 10 mm thickness. The chemical composition of the Nd-Fe-B is summarised in the Table 1.

The physicochemical properties of the Nd-Fe-B Magnet [33–38] can be seen in the Table 2.

Thermal diffusivity (κ) was calculated with Eq. 1 [14, 39, 40].

$$\kappa = \frac{\beta}{\rho * C_p} \quad (1)$$

The surfaces of the samples were polished before the laser processing (pre-treatment). The polishing process was carried out in three successive steps. First step was a subsequent grinding process with silicon carbide papers of P400, P600 and P1200. The next step was a sequential polishing via polycrystalline diamond pastes of 6 μm , 3 μm and 1 μm . The last step was a mirror polishing using a colloidal silica gel dissolution that consisted of 50% in volume of silica gel (0.04 μm of grain size) and 50% in volume of distilled water. All polishing consumables and items supplied by *Struers*. Note a cleaning process was conducted after each polishing process. The

Table 2 Nd-Fe-B Physic-chemical properties. *Value calculated using Eq. (1). [‡] Value of the steel. [°] Value of 316 stainless steel

Property	Value
Specific Heat Capacity (C _p) [33, 34]	0.440 J/(g*°K)
Thermal Conductivity (β) [34]	0.090 J/(K*cm*s)
Density (ρ) [34, 36]	7.500 g/cm ³
Thermal Diffusivity* (κ)	0.027cm ² /s
Absorption coefficient (α) [37] [‡]	52.0 μm ⁻¹
Melting Temperature (T _m) [35]	1289 K
Vaporisation Temperature (T _e) [35]	3343 K
Standard Temperature (T _o)	296 K
Melting Enthalpy (ΔH _m) [37] [‡]	272 J/g
Evaporation Enthalpy (ΔH _e) [37]	6095 J/g
Molar Mass (M) [36]	211 mol/g
Reflectivity (R) [38] [°]	70%

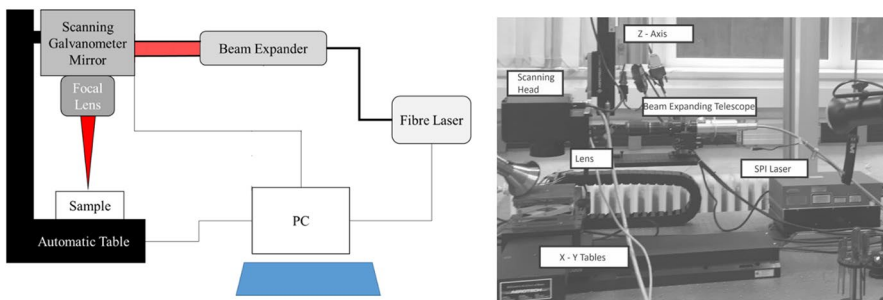


Fig. 1 Schematic drawing and view of the laser equipment

cleaning treatment was comprised of a first cleaning with commercial detergent and rinsing with fresh water, then an isopropanol spraying and, finally a fast drying with dryer.

Laser facility and parameters

The laser equipment was formed of an infrared (IR) fibre laser, an optical system and three axes automatic table. The IR fibre laser model was a *SPI Laser (UK) G3 20 W nanosecond pulsed fibre laser*. The optical system consisted of a *Linos (Qioptiq) 2-8x, 1064 nm beam expander*, a *Nutfield Extreme-15-YAG scanning galvanometer* controlled using *SAMLight v3.05 software (SCAPS GmbH)*, and a *Linos Ronar F-Theta focal lens*. The three axes computer controlled table was supplied by *Aero-tech Limited (UK)*. Figure 1 illustrates a schematic drawing of this equipment.

The IR laser fibre has a wavelength (λ) 1064 nm, near TEM₀₀ mode with beam quality $M^2=2.1$. The working modes of the laser are continuous wave (CW) and pulsed mode. The available pulse lengths of the laser (τ) were from 9ns to 200ns and its Pulse Repetition Frequency (PRF) was from 1 to 500 kHz. The laser has a maximum average power (P_m) of 22 W and maximum pulse energy (E_{pm}) of 880μJ. The maximum average power was measured after the beam expander with an Ophir laser power meter system, using a *30 A-N-SH ROHS head* and *Nova II display*. The

power was measured during 60s. Maximum pulse energy was calculated with the Eq. (2) [41].

$$E_{pm} = \frac{P_m}{PRF} \quad (2)$$

The laser beam was addressed to the sample surfaces with the following optical system: The beam expander widened the diameter of the laser raw beam (D_R) to 5.7 mm and also guided the laser beam to scanning galvanometer mirror. The laser beam was addressed to the f-theta focussing lens via the scanning galvanometer mirror. This device controlled the displacement of the laser beam on the sample surfaces and the scan rate of the laser beam (SR) could be varied from 0.01 mm/s to 20,000 mm/s. The focal lens had a focal length (FL) of 100 mm. Note, the samples were placed on the three axes automatic table and the beam expander was manually set.

In this study, the laser device was working in pulsed mode with $\tau=200\text{ns}$, τ , $PF=25$ kHz and with straight line scanning. The laser beam was focused on the surfaces of the samples. The theoretical laser beam diameter ($d_{o(\text{Theo})}$) was 51 μm , calculated using Eq. 3 [26, 27, 42] and the values of the Table 3 for each parameters. This value was estimation form theoretical values.

$$d_{o(\text{Theo})} = \frac{4 * FL * \lambda * M^2}{\pi * D_R} \quad (3)$$

The laser was scanned over the sample surfaces to achieve single pulse exposures. The distance between pulses (d_t) was set to avoid any possible overlapping of the pulses, which was 300 μm . The SR was 7500 mm/s, calculated using Eq. 4:

$$SS = d_t * PF \quad (4)$$

E_p was varied from 5 μJ to 696 μJ in this work. E_p were estimated with the Eq. (5) [41] and the average power (P_{ave}) measurements after galvanometer mirror scanner.

$$E_p = \frac{P_{ave}}{PRF} \quad (5)$$

Maximum E_p was lower than E_{pm} because the scanning galvanometer mirror reduced the power at 20%.

The selected laser parameters for this study are summarised in the Table 3.

Analysis techniques

The surface morphologies of the samples were evaluated by mean of an *Olympus BH2-UMA optical light microscope*. The optical microscopy pictures were obtained at 20X magnification with *DinoCapture 2.0* software.

Table 3 Selected laser parameters in this study

Parameter	Value
λ (μm)	1064
τ (ns)	200
TEM	00
FL (mm)	100.00
D_R (mm)	5.7
M^2	2.1
SS (mm/s)	7500
d_t (μm)	300
$d_{o(\text{Theo})}$ (μm)	51
PRF(kHz)	25
Atmosphere	Air
Number of pulses exposed (N)	1
E_p (μJ)	5, 61, 130, 201, 278, 359, 449, 529, 611 and 696

The topography of the samples was analysed with the *Bruker ContourGT* optical profiler. The assessing of the optical profilometry was carried out with green light, at 27.5X magnification.

Results and Discussion

Surface morphology

Figure 2 shows the images of the laser processed samples and mirror polished surface (Fig. 2.a). The laser pulses at $\geq 130\mu\text{J}$ created dimples with morphologies that were irregular circumference (Fig. 2.b-d). This morphology can be due to the magnetic field of the material. The melting and evaporation of the material are usually the mechanisms that generate the dimples on metals for IR laser exposures [16]. These thermal processes are commonly featured by the ablation mechanism of hydrodynamic expansion for nanosecond pulse laser. The dimples of these ablation mechanisms are characterised by having melted material around the laser exposed area. The hydrodynamic expansion causes the melted material to mass on the dimple edges, which forms the circular shape of the dimple [43]. The melted material was accumulated both on the edges as well as the interior of the dimples (Fig. 2.b-d). This indicates that an external force had limited the hydrodynamic movements of the liquid material. With the exception of the gravity and magnetic field of the Earth, the magnetism of the Nd-Fe-B magnet was the only unique force applied on the liquid material. This force was responsible for the ejected material absence around the dimples and the irregular dimple forms because it retained the liquid material inside the laser exposed zone. This also indicated that the molten magnetic material is still being magnetically active [23, 25].

Some characteristics of the dimples were different according to E_p . The dimples at $\geq 210\mu\text{J}$ had ejected material outside shot area (Fig. 2c-d.). This can indicate that

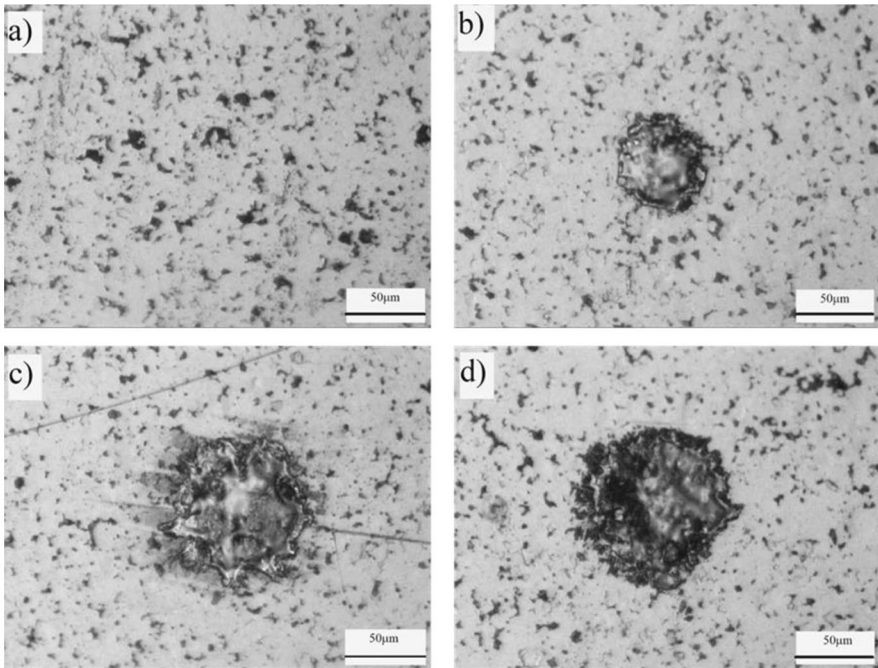


Fig. 2 The micrographic pictures of the (a) mirror polished surface and dimple via single pulse at (b) 130 μ J, (c) 449 μ J and (d) 696 μ J

these dimples are created by the ablation mechanism called as explosion phase. This mechanism is the nucleation and subsequent growth of a bubble that consists of evaporated material surrounded by liquid. The gas material causes pressure on the melted material. If this pressure is sufficiently elevated, the bubble can explode. This explosion ejects the molten material outside of the laser treated area [16, 43, 44]. The ejected material is absent on the dimples at 134 μ J (Fig. 2.b.), which indicates that another mechanism produces these dimples, which is surface vaporisation. This ablation mechanism is featured by the transformation of the liquid to gas in a liquid-gas interface that is often called the Knudsen layer. Although the escape velocity distribution of evaporated material in the liquid layer initially is non-equilibrium, this distribution becomes equilibrium with time [16, 43]. The dissimilar ablation mechanism for dimples at 134 μ J with respect to the dimples created at other E_p is because the energy fluence necessary for each mechanism is different. Usually, the explosion phase requires more energy fluence than surface vaporisation [16].

The ejected material was so close to the dimple (Fig. 2c-d.) due to the magnetic force of the sample. This material can generally be found within a certain distance of the laser hit area [45]. This distance is reduced by the magnetic force of the material because the molten material is magnetic active [23, 25]. The Lorentz force can be opposite direction to the ejection force created by explosion phase. The distance between ejected material and the dimple was lower than expected distance.

The width of the dimples (W), defined as the diameter of all the area treated by the laser pulse, was widened with the increment of E_p , as can be in the graph of Fig. 3. This is because the energy spatial distribution is Gaussian like [26].

The focused laser beam diameter (d_o) and the pulse energy threshold for melting process ($E_{th-melting}$) were $53.8 \pm 13.2 \mu\text{m}$ and $54.889 \pm 0.004 \mu\text{J}$, respectively. $E_{th-melting}$ represented the minimum laser energy necessary to melt the magnet. These values were estimated via Eq. 6 [26, 28] and the liner regression method of the Fig. 3.b. graph data.

$$W^2 = d_o^2 * \ln(E_p) - d_o^2 * \ln(E_{th-melting}) \quad (6)$$

d_o was slightly larger than to $d_{o(\text{Theo})}$ ($51 \mu\text{m}$) because the ejected material increases W . Liquid material is ejected outside the pulse zone through explosion phase, which produces an increasing of the ablation rate [44]. This enhancement of the ablation rate means that the dimples are deeper and wider than in the case of the normal situation of evaporation. This causes that the growth rate of the W with the increasing of E_p is greater than the theoretical value that was $d_{o(\text{Theo})}$.

The experimental energy fluence threshold (ϕ_{th}) was 2.4 J/cm^2 calculated through Eq. 7.

$$\phi_{th} = \frac{4 * E_{th}}{\pi * d_o^2} \quad (7)$$

ϕ_{th} was higher than theoretical energy fluence threshold for melting ($\phi_{th(\text{Theo-melting})}$) that was 1.334 J/cm^2 , which was estimated via Eq. 8 [15, 40].

$$\phi_{th(\text{Theo-melting})} = \frac{\rho * (c_p * (T_m - T_o) + \Delta H_m)}{1 - R} * (\sqrt{\kappa * \tau} + \frac{1}{\alpha}) \quad (8)$$

This is due to the magnetic forces of the samples that can reduce W . As mentioned, the electromagnetic forces produced by solid material can attract the melted material to the centre of the laser impacted zone [25]. This produces a contraction of the melting material, which in turn narrows W . This is observed in the higher experimental energy fluence threshold than that that for theoretical case.

Topography

The topography of the dimples consists of a valley surrounded by a crest, as can be observed in Fig. 4. The valley is formed by the ablation of the material via the evaporation of metallic material and the movement of the molten material to outside laser shot area [18, 24]. The crest around valley is created by mean of the accumulation of the liquid material on dimple rim and after its subsequent, fast, re-solidification. The pressure of the evaporated material on the molten displaces the liquid material to edge of the dimple [22, 24]. The shape of the dimples is a spherical cap that is commonly called U-type [29–32]. This shape is due to only the Gaussian peak of the laser beam having sufficient energy to ablate the material [32].

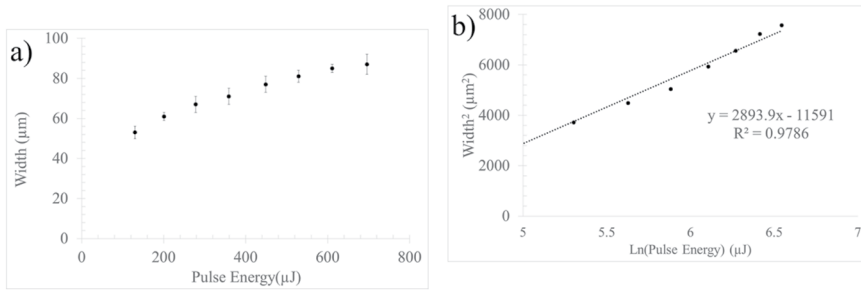
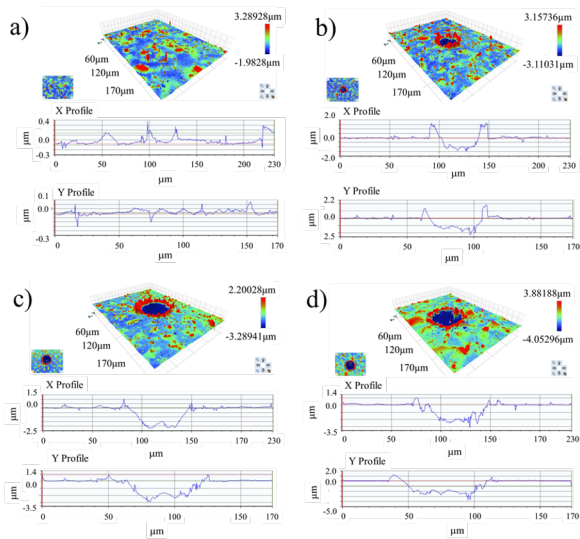


Fig. 3 Graphs of the pulse energy influence on width, (a) width as function pulse energy and (b) width square vs. pulse energy natural logarithm

Fig. 4 The 3D images and profiles of the (a) mirror polished surface and the dimple via single pulse at (b) 130μJ, (c) 449μJ and (d) 696μJ



The graphs of Fig. 5 show the diameter of the dimple (d) according to E_p . d is defined as the diameter of the ablated area. Increasing E_p also increased the d because of the Gaussian energy spatial distribution in laser beam [10, 32]. d_o (focused laser beam diameter) and E_{th} (minimum laser energy to ablate the magnetic material) were estimated using Eq. 9 [10, 28] while ϕ_{th} (minimum laser energy fluence to ablate the magnet) was calculated using Eq. 7.

$$d^2 = d_o^2 * \ln(E_p) - d_o^2 * \ln(E_{th}) \tag{9}$$

d_o was found to be 41 μm, lower than $d_{o(Theo)}$ (51 μm), whose dissimilarity was 20%. This is because the magnetic forces of the samples that can diminish d_o [23–25], as previously mentioned. In respect of ϕ_{th} , its value was 3.756 J/cm² that was lower than $\phi_{th(Theo-evaporating)}$ (13.190 J/cm²). $\phi_{th(Theo-evaporating)}$ was the minimum laser energy fluence to ablate the material, which was calculated through Eq. 10 [15, 27, 40]:

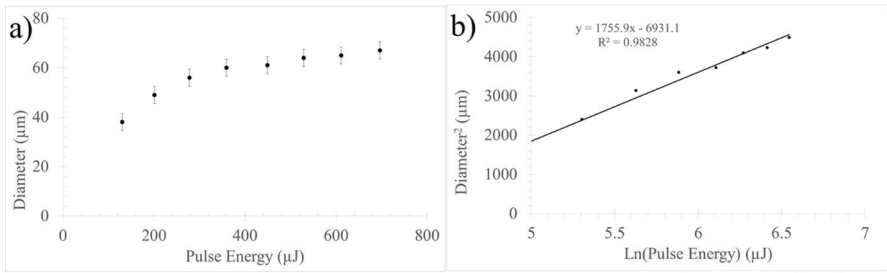


Fig. 5 Graphs of the pulse energy influence on diameter, (a) diameter as function pulse energy and (b) diameter square vs. pulse energy natural logarithm

$$\phi_{th(\text{Theo-evaporating})} = \frac{\rho * (c_p * (T_e - T_m) + \Delta H_e + c_p * (T_m - T_o) + \Delta H_m)}{1 - R} * (\sqrt{\kappa * \tau} + \frac{1}{\alpha}) \quad (10)$$

The dissimilarity of the values is due to two reasons. The first reason is the reflectivity, R , of the mirror polished surface is different to the values of R from literature. The surface roughness can diminish the R of the samples because the laser beam can be scattered with >180 degrees by peaks and valleys of the surface. Reflected laser radiations can impact again on the surface, which improves the absorption of the laser beam by material [14, 28]. Secondly, there is a greater rate of ablation in the explosive phase than that for surface vaporisation. The explosion of the bubble increases the amount of the removed material due to the ejection of the molten material, which is characteristic of the explosion phase [44]. The explosion phase mechanism thus needs less energy than normal vaporisation to produce a similar ablation rate. $\phi_{th(\text{Theo-evaporating})}$ was calculated according to normal evaporation and therefore, this value is greater than experimental value. The increasing of E_p deepened the cell, as can be seen in the graphs of Fig. 6. This is due to the amount of the ablated material being proportional to pulse energy [18]. Energy depth penetration (l) (the depth to which absorbed laser energy is transferred by thermal processes) and pulse energy threshold (E_{th}) (minimum pulse energy to produce a dimple with observable depth) for this case, were estimated using the graph of Fig. 6.b. and Eq. 11 [18, 40], where D is the depth of the cell.

$$D = l * \ln(E_p) - l * \ln(E_{th}) \quad (11)$$

l and E_{th} were $0.623 \mu\text{m}$ and $16.449 \mu\text{J}$, respectively. l is the same as the theoretical energy depth penetration (l_{Theo}) for a geometric factor (ξ) of 1.3. This factor was calculated with Eq. 11 [17, 26, 27].

$$l_{\text{Theo}} = \sqrt{\xi * \tau * \kappa} + \frac{1}{\alpha} \quad (11)$$

Figure 7 shows the graph of average roughness as function of the pulse energy. Mirror polished surfaces had an average roughness of $0.066 \pm 0.003 \mu\text{m}$. All surfaces

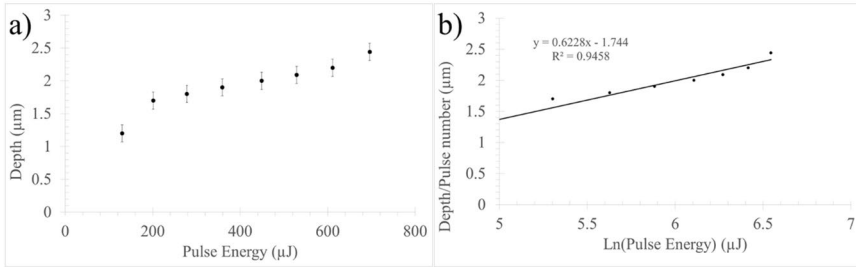
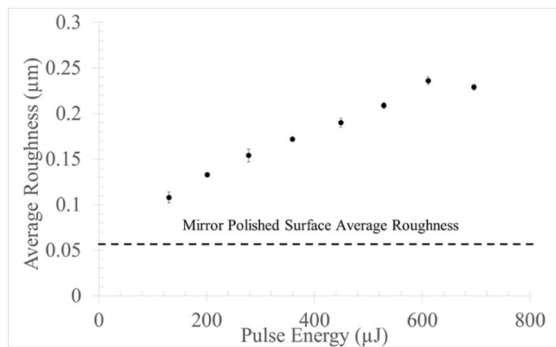


Fig. 6 Graphs of the pulse energy influence on depth, (a) pulse energy vs. depth and (b) pulse energy natural logarithm vs. depth

Fig. 7 Graphs of the average roughness as function of pulse energy



with dimples were rougher than the original surfaces. The generation of a dimple on polished surfaces increases the relief, which rises the average roughness of the samples. The average roughness rose with the increment of the pulse energy because this feature of the samples is proportional to dimple size. Sample relief is proportional to dimple size and, it is in turn risen with the increment of E_p . The rate of the ablation is greater at higher E_p [18]. Thus, average roughness is proportional to E_p .

Conclusions

The present work shows that the melted material of the NdFeB alloy is still magnetically active. Although this effect slightly impoverishes the quality of the textures, the dimples have an acceptable shape. The magnetic activity of the molten material indicates that this magnet can be designed by mean of other laser processes as, laser selective melting and laser additive manufacturing.

In addition, this study provides important information about the influence of the pulse energy on cell characteristics (W , d , D and average roughness), which was characterised through the determination of the laser beam-material interaction factors (I , E_{th} and ϕ_{th}). The quantification of these factors can allow the design of features of the textures generated by single pulses on NdFeB alloy. This can therefore allow the

creation of functionalised NdFeB alloy surfaces with desired properties, which can have numerous applications, e.g. in manufacturing and electronic engineering.

Author contributions All authors contributed to the study conception and design. Material preparation, data collection and analysis were performed by Juan Ignacio Ahuir-Torres. The first draft of the manuscript was written by Juan Ignacio Ahuir-Torres and Juan Ignacio Ahuir-Torres, and all authors commented on previous versions of the manuscript. All authors read and approved the final manuscript.

Funding The authors declare that no funds, grants, or other support were received during the preparation of this manuscript.

Data Availability The datasets generated during and/or analysed during the current study are available in the manuscript.

Declarations

Conflict of interest There are no conflicts of interest.

Open Access This article is licensed under a Creative Commons Attribution 4.0 International License, which permits use, sharing, adaptation, distribution and reproduction in any medium or format, as long as you give appropriate credit to the original author(s) and the source, provide a link to the Creative Commons licence, and indicate if changes were made. The images or other third party material in this article are included in the article's Creative Commons licence, unless indicated otherwise in a credit line to the material. If material is not included in the article's Creative Commons licence and your intended use is not permitted by statutory regulation or exceeds the permitted use, you will need to obtain permission directly from the copyright holder. To view a copy of this licence, visit <http://creativecommons.org/licenses/by/4.0/>.

References

1. Yang, Y., Walton, A., Sheridan, R., Güth, K., Gauß, R., Gutfleisch, O., Buchert, M., Steenari, B.-M., Van Gerven, T., Jones, P.T.: REE recovery from end-of-life NdFeB permanent magnet scrap: a critical review. *J. Sustainable Metall.* **3**(1), 122–149 (2017)
2. Yanfeng, L., Minggang, Z., Anhua, L., Haibo, F., Wei, H.U.A.N.G.S., An, L., Yan, D.: Relationship between controllable preparation and microstructure of NdFeB sintered magnets. *J. Rare Earths.* **32**(7), 628–632 (2014)
3. YANG, Z.H.A.N.G.H., X.-p., B.A.I.S., Ke, C., Fei, Y.: Toughness of sintered NdFeB magnets. *J. Iron Steel Res. Int.* **13**, 494–499 (2006)
4. Mitchell, P.: Corrosion protection of NdFeB magnets. *IEEE Trans. Magn.* **26**(5), 1933–1935 (1990)
5. Gao, J., Volkmann, T., Roth, S., Löser, W., Herlach, D.: Phase formation in undercooled NdFeB alloy droplets. *J. Magn. Magn. Mater.* **234**(2), 313–319 (2001)
6. Yan, G., Williams, A., Farr, J., Harris, I.: The effect of density on the corrosion of NdFeB magnets. *J. Alloys Compd.* **292**(1–2), 266–274 (1999)
7. Yu, L., Wen, Y., Yan, M.: Effects of Dy and Nb on the magnetic properties and corrosion resistance of sintered NdFeB. *J. Magn. Magn. Mater.* **283**(2–3), 353–356 (2004)
8. Etsion, I.: State of the art in laser surface texturing. *J. Trib.* **127**(1), 248–253 (2005)
9. Etsion, I.: Laser surface texturing and applications. *Recent developments in wear prevention, friction and lubrication:137–158.* (2010)
10. Puoza, J.C., Hua, X., Liu, Q., Kang, Z., Zhang, P.: Manufacturing of micro-textures on metals by nanosecond laser micromachining. *Adv. Mater. Process. Technol.* **4**(1), 86–99 (2018)
11. Chilamakuri, S.K., Bhushan, B.: Optimization of asperities for laser-textured magnetic disk surfaces. *Tribol. Trans.* **40**(2), 303–311 (1997)

12. Wahab, J., Ghazali, M., Yusoff, W., Sajuri, Z.: Enhancing material performance through laser surface texturing: A review. *Trans. IMF.* **94**(4), 193–198 (2016)
13. Tam, A., Pour, J., Nguyen, T., Krajinovich, D., Baumgart, P., Bennett, T., Grioropoulos, C.: Experimental and theoretical studies of bump formation during laser texturing of Ni-P disk substrates. *IEEE Trans. Magn.* **32**(5), 3771–3773 (1996)
14. Brown, M.S., Arnold, C.B.: Fundamentals of laser-material interaction and application to multiscale surface modification. In: *Laser precision microfabrication*, pp. 91–120. Springer (2010)
15. Domke, M., Nobile, L., Rapp, S., Eiselen, S., Sotrop, J., Huber, H.P., Schmidt, M.: Understanding thin film laser ablation: The role of the effective penetration depth and the film thickness. *Phys. Procedia.* **56**, 1007–1014 (2014)
16. Wu, B., Özel, T.: *Micro-Laser Processing. Micro-Manufacturing: Design and Manufacturing of Micro-Products*: 159–195. (2011)
17. Xiao, S., Schöps, B., Ostendorf, A.: Selective ablation of thin films by ultrashort laser pulses. *Phys. Procedia.* **39**, 594–602 (2012)
18. Ahuir-Torres, J., Arenas, M., Perrie, W., De Damborenea, J.: Influence of laser parameters in surface texturing of Ti6Al4V and AA2024-T3 alloys. *Opt. Lasers Eng.* **103**, 100–109 (2018)
19. Vadillo, J., Fernandez Romero, J., Rodriguez, C., Laserna, J.: Effect of plasma shielding on laser ablation rate of pure metals at reduced pressure. *Surface and Interface Analysis: An International Journal devoted to the development and application of techniques for the analysis of surfaces, interfaces and thin films* 27 (11):1009–1015. (1999)
20. Sasi, R., Subbu, S.K., Palani, I.: Performance of laser surface textured high speed steel cutting tool in machining of Al7075-T6 aerospace alloy. *Surf. Coat. Technol.* **313**, 337–346 (2017)
21. Lee, D.H., Kim, T.H., Jung, E.C., Yun, J.-I.: Shielding effect of laser-induced plasma in glass: pulse-to-pulse evolution of nitrogen and analyte emission lines. *Appl. Phys. A.* **104**(3), 863–869 (2011)
22. Cha, D., Axinte, D., Billingham, J.: Geometrical modelling of pulsed laser ablation of high performance metallic alloys. *Int. J. Mach. Tools Manuf.* **141**, 78–88 (2019)
23. Balamurugan, S., Manikandan, C.B., Balamurugan, P.: A study on magnetic field assisted laser percussion drilling and its effect on surface integrity. *Archives of Materials Science and Engineering* 94 (1). (2018)
24. Baumgart, P., Krajinovich, D., Nguyen, T., Tam, A.: A new laser texturing technique for high performance magnetic disk drives. *IEEE Trans. Magn.* **31**(6), 2946–2951 (1995)
25. Ho, C.-C., Tseng, G.-R., Chang, Y.-J., Hsu, J.-C., Kuo, C.-L.: Magnetic-field-assisted laser percussion drilling. *Int. J. Adv. Manuf. Technol.* **73**(1), 329–340 (2014)
26. Mannion, P., Magee, J., Coyne, E., O’connor, G., Glynn, T.: The effect of damage accumulation behaviour on ablation thresholds and damage morphology in ultrafast laser micro-machining of common metals in air. *Appl. Surf. Sci.* **233**(1–4), 275–287 (2004)
27. Włodarczyk, K.L., Ardron, M., Waddie, A.J., Dunn, A., Kidd, M.D., Weston, N.J., Hand, D.P.: Laser microsculpting for the generation of robust diffractive security markings on the surface of metals. *J. Mater. Process. Technol.* **222**, 206–218 (2015)
28. Mustafa, H., Mezera, M., Matthews, D.T.A., Römer, G.: Effect of surface roughness on the ultrashort pulsed laser ablation fluence threshold of zinc and steel. *Appl. Surf. Sci.* **488**, 10–21 (2019)
29. Nanbu, T., Ren, N., Yasuda, Y., Zhu, D., Wang, Q.J.: Micro-textures in concentrated conformal-contact lubrication: effects of texture bottom shape and surface relative motion. *Tribol. Lett.* **29**(3), 241–252 (2008)
30. Gropper, D., Wang, L., Harvey, T.J.: Hydrodynamic lubrication of textured surfaces: a review of modeling techniques and key findings. *Tribol. Int.* **94**, 509–529 (2016)
31. Shiman, O., Gerbreder, V., Sledevskis, E., Paskevics, V.: Electron beam induced surface modification of amorphous Sb₂Se₃ thin film. *J. Non-cryst. Solids.* **358**(8), 1153–1156 (2012)
32. Zhan, X., Liu, Y., Yi, P., Jia, D., Xiao, P.: Study on the influence of scanning strategy on the morphology of laser micro-dimple texturing. In: *Tenth International Conference on Information Optics and Photonics*, International Society for Optics and Photonics, p 109640P (2018)
33. Raulf, K., Pretz, T.: Model-Based Comparison of Recycling Processes for Grinding Slurries from NdFeB-Magnet Production. *J. Sustainable Metall.* **3**(1), 150–167 (2017)
34. MatWeb, MatWeb:LLC
35. Tamas M., Stanescu C., Ene D.: Bending Behavior Assessment of NdFeB Magnet Based Samples. (2015)
36. product, A.E.: CAS No. 918106-59-9, vol. MFC02091729. American Elements product, Los Angeles, United States of America (2015)

37. Le Harzic, R., Breitling, D., Weikert, M., Sommer, S., Föhl, C., Valette, S., Donnet, C., Audouard, E., Dausinger, F.: Pulse width and energy influence on laser micromachining of metals in a range of 100 fs to 5 ps. *Appl. Surf. Sci.* **249**(1–4), 322–331 (2005)
38. Wisse, M., Marot, L., Eren, B., Steiner, R., Mathys, D., Meyer, E.: Laser damage thresholds of ITER mirror materials and first results on in situ laser cleaning of stainless steel mirrors. *Fusion Eng. Des.* **88**(5), 388–399 (2013)
39. Zhou, J., Shen, H., Pan, Y., Ding, X.: Experimental study on laser microstructures using long pulse. *Opt. Lasers Eng.* **78**, 113–120 (2016)
40. Wu, B., Liu, P., Wang, X., Zhang, F., Deng, L., Duan, J., Zeng, X.: Effect of laser absorption on picosecond laser ablation of Cr12MoV mold steel, 9Cr18 stainless steel and H13A cemented carbide. *Opt. Laser Technol.* **101**, 11–20 (2018)
41. Jiang, D., Alsagri, A.S., Akbari, M., Afrand, M., Alrobaian, A.A.: Numerical and experimental studies on the effect of varied beam diameter, average power and pulse energy in Nd: YAG laser welding of Ti6Al4V. *Infrared Phys. Technol.* **101**, 180–188 (2019)
42. Sola, D., Conde, A., García, I., Gracia-Escosa, E., De Damborenea, J.J., Peña, J.I.: Microstructural and wear behavior characterization of porous layers produced by pulsed laser irradiation in glass-ceramics substrates. *Materials.* **6**(9), 3963–3977 (2013)
43. Marla, D., Bhandarkar, U.V., Joshi, S.S.: A model of laser ablation with temperature-dependent material properties, vaporization, phase explosion and plasma shielding. *Appl. Phys. A.* **116**(1), 273–285 (2014)
44. Song, K.H., Xu, X.: Explosive phase transformation in excimer laser ablation. *Appl. Surf. Sci.* **127**, 111–116 (1998)
45. Fishburn, J., Withford, M., Coutts, D., Piper, J.: Study of the fluence dependent interplay between laser induced material removal mechanisms in metals: Vaporization, melt displacement and melt ejection. *Appl. Surf. Sci.* **252**(14), 5182–5188 (2006)

Publisher's Note Springer Nature remains neutral with regard to jurisdictional claims in published maps and institutional affiliations.